ACES Asian Chemical Editorial Society

DOI: 10.1002/asia.201800125

CHEMISTRY AN ASIAN JOURNAL Full Paper

Single-Atom Catalysts

Designed Precursor for the Controlled Synthesis of Highly Active Atomic and Sub-nanometric Platinum Catalysts on Mesoporous Silica

Sudipta De,[a] Maria V. Babak,[b] Max J. Hülsey,[a] Wee Han Ang,*[b] and Ning Yan*[a]

Abstract: The development of new methods to synthesize nanometric metal catalysts has always been an important and prerequisite step in advanced catalysis. Herein, we design a stable nitrogen ligated Pt complex for the straightforward synthesis by carbonization of uniformly sized atomic and sub-nanometric Pt catalysts supported on mesoporous silica. During the carbonization of the Pt precursor into active Pt species, the nitrogen-containing ligand directed the decomposition in a controlled fashion to maintain uniform sizes of the Pt species. The nitrogen ligand had a key role to stabilize the single Pt atoms on a weak anchoring support like silica. The Pt catalysts exhibited remarkable activities in the hydrogenation of common organic functional groups with turnover frequencies higher than in previous studies. By a simple post-synthetic treatment, we could selectively remove the Pt nanoparticles to obtain a mixture of single atoms and nanoclusters, extending the applicability of the present method.

Introduction

Precise control of active catalytic sites plays a crucial role in designing highly effective heterogeneous catalytic systems. In particular, the size of the metal species, such as single sites, metal nanoparticles (NPs), or bulk state, directly affects their catalytic activities.[1] Development of synthetic strategies that can control the nature of the active catalytic centers, switching from single sites to nanostructure ensembles, is therefore both an important and yet challenging task. Conventional methods, such as sol-gel and wet impregnation, are widely accepted owing to their inherent simplicity in employing simple metal salt precursors, such as nitrates, chlorides, and acetates. However, these methods do not normally provide satisfactory control over particle size. It is often observed that the thermal treatment during syntheses or catalytic processes induce aggregation of the active species to form large NPs (>5 nm), resulting in a decrease of catalytic activity.[2] A plausible way to address this problem is the employment of stable metal complexes as the catalyst precursors, as these compounds have higher thermal stabilities than those of simple metal salts, and would gradually decompose upon increasing the temperature, allowing uniform formation of small metal NPs. Indeed, several organometallic complexes with unique properties have been employed as metal precursors to form structured metal NPs with controlled size.[3] Mononuclear organometallic complexes have also been demonstrated as promising precursors to produce catalytic active sites as metal clusters.[4]

Nitrogen ligand containing transition metal (e.g., Fe, Co, Ni) complexes were recently employed as precursors that could effectively produce single-atom active sites after pyrolysis over suitable supports.[5] In all cases, the M-N-C (M typically refers to transition metals) structure was retained in the catalysts owing to the strong M–N bond. As a result, high metal loading (up to 4 wt%) could be obtained without considerable agglomeration of single active sites. Similarly, the metal–organic framework (MOF) approach was applied to synthesize single-site catalysts, where carbonization at high temperature produced porous N-doped carbon support with anchoring groups to stabilize the metal atoms.[6] It was proven that the M-N-C catalysts had comparative electrochemical performances with that of the commercial Pt/C catalyst owing to the presence of conductive M–N_x coordination spheres. N-doped metal catalysts have also shown improved activities in different organic transformations. For example, the Co-N-C system showed superior catalytic activity in coupling reactions owing to electron-rich metal sites adjacent to the N atoms.[5a] It was recently reported that the M–N species offered favorable adsorption of reactants on the active sites, facilitating product formation.[7]

Several metal oxides including Fe_2O_3,[8] Al_2O_3,[9] CeO_2,[10] TiO_2,[11] ZnO,[12] and nitrides such as C_3N_4[13] and TiN,[14] as well as heteropoly acids[15] have been used to stabilize single metal

[a] Dr. S. De, M. J. Hülsey, Prof. Dr. N. Yan
Department of Chemical and Biomolecular Engineering
National University of Singapore
4 Engineering Drive 4, 117585, Singapore (Singapore)
E-mail: ning.yan@nus.edu.sg

[b] Dr. M. V. Babak, Prof. Dr. W. H. Ang
Department of Chemistry
National University of Singapore
3 Science Drive 2, 117543 Singapore (Singapore)
E-mail: ang.weehan@nus.edu.sg

Supporting information and the ORCID identification number(s) for the author(s) of this article can be found under https://doi.org/10.1002/asia.201800125.

atoms and sub-nanoclusters owing to the presence of anchoring sites or lattice defects. However, in spite of high surface area, it is still challenging to stabilize single-atom catalysts (SACs) and sub-nanoclusters on silica, presumably owing to its weak metal–support interaction. Herein, we report a stable mononuclear Pt complex based on a pyridine-based tridentate ligand (tris(*tert*-butyl)terpyridine or TBTP), which produced uniformly sized nanometric Pt species along with single Pt atoms over mesoporous SBA-15 silica. The bulky TBTP ligand is designed to protect the Pt species and provides high thermal stability owing to the presence of strong Pt–N bonds. As a result, the decomposition of the Pt complex occurred in a well-controlled fashion to yield an increased population of catalytically active single Pt atoms.

Results and Discussion

We followed a simple two-step procedure to synthesize the mononuclear Pt complex ([Pt(*t*Bu$_3$tpy)Cl]Cl or Pt(TBTP); see the Supporting Information), and the product was characterized by using ESI-MS analysis (Figure 1 (a)), which showed a strong molecular ion peak at $m/z = 632.2$. Thermogravimetric analysis (Figure 1 (b)) revealed that the Pt complex was stable up to 350 °C before starting to decompose and the weight of the residue became stable from 450 °C onwards. Supported Pt catalysts (designated as *x* Pt-SBA-15-*T*, where *x* is Pt loading and *T* is treatment temperature) with different metal loadings were prepared by the wet impregnation method. To obtain information on the formation of Pt species, temperature-programmed desorption mass spectrometry (TPD-MS), elemental analysis (EA), and X-ray photoelectron spectroscopy (XPS) studies were conducted with 1.5 wt% Pt(TBTP) complex supported on SBA-15. The TPD-MS profile (Figure 2) shows the loss of carbon species in the form of CO and CO_2 at different temperatures. Presumably, the silica support provided a trace amount of oxygen for carbon oxidation. Up to 600 °C, a significant amount of carbon was retained and very little nitrogen loss was observed. XPS results (Figure S1 in the Supporting Information) show that the oxidation state of Pt remained the same as in the Pt precursor after treatment at 400 °C. For the treatment temperature 500 °C, however, Pt species exhibited different oxidation states owing to partial removal of the ligand and formation of clusters/NPs. The nitrogen content also decreased upon increasing the treatment temperature from 400 °C to 500 °C. In both samples, nitrogen species were observed in the form of imine bonding modes (C=N-C). Combination of TPD-MS, EA, and XPS studies revealed that both carbon and nitrogen species were partly retained on the support, which stabilized the positively charged Pt single atoms and close to zero-valent small clusters (see below).

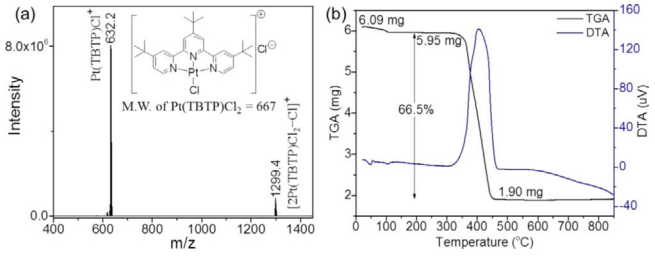

Figure 1. (a) ESI-MS spectrum and (b) thermogravimetric/differential thermal analysis (TGA/DTA) profile of Pt(TBTP)Cl$_2$ complex.

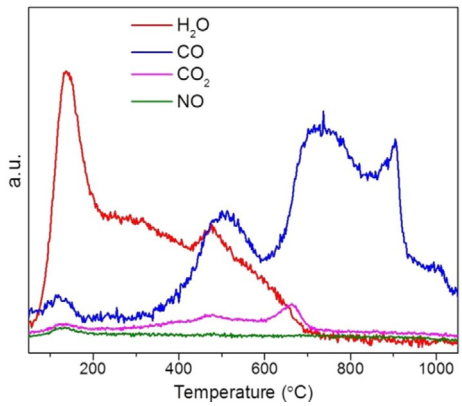

Figure 2. TPD-MS profile of Pt complex supported on SBA-15.

Initial characterization results showed that the heat treatment of the supported Pt sample (0.2 wt% Pt) at 500 °C produces a mixture of single atoms and small clusters (or NPs) as observed from the IR spectra (Figure 3 (a)). Two characteristic peaks located at 2090 cm^{-1} and 2075 cm^{-1} can be assigned as linearly adsorbed CO on Pt single atoms and clusters (or NPs), respectively. XPS results also supported this observation as Pt moieties existed in a partially oxidized state (Figure S2 (a) in the Supporting Information). When the temperature was increased to 600 °C, the IR peak at 2090 cm^{-1} shifted to 2087 cm^{-1} with concomitant peak broadening, presumably owing to the combination of the two peaks (Figure 3 (b)), indicating the higher heterogeneity of Pt species. The metallic character also increased at higher temperatures, which could

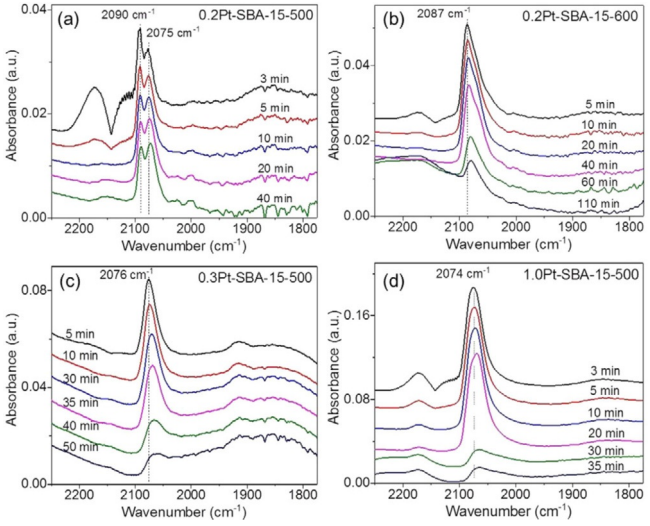

Figure 3. IR spectra of CO adsorbed on different samples: (a) 0.2 Pt-SBA-15-500, (b) 0.2 Pt-SBA-15-600, (c) 0.3 Pt-SBA-15-500, (d) 1.0 Pt-SBA-15-500. Spectra were taken under N_2 flow after CO adsorption.

possibly decrease the percentage of single-atom species. However, NPs were hardly observed for any of these samples from TEM (Figure 4(c) and Figure S4(a, b) in the Supporting Information). When the loading was increased to 0.3 wt%, the IR peak

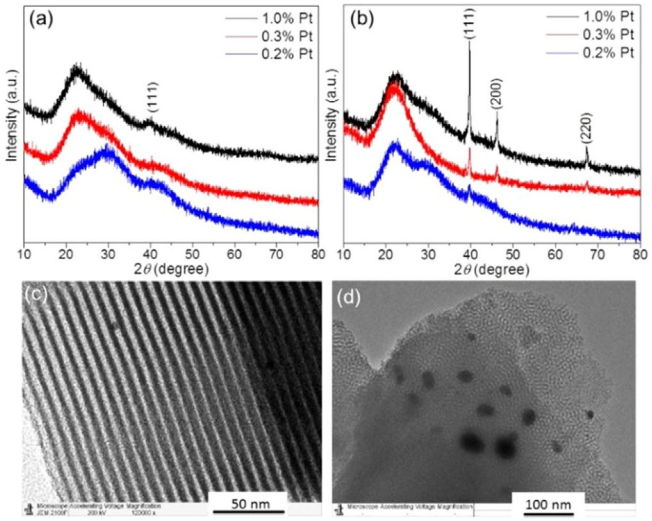

Figure 4. XRD spectra of Pt-SBA-15 materials at different loadings prepared from (a) TBTP complex and (b) H_2PtCl_6 precursors. TEM images of (c) 0.2 Pt-SBA-15-500 and (d) 0.2 Pt-SBA-15-500-C.

at 2090 cm^{-1} was totally abrogated and the peak at 2076 cm^{-1} became broader and unsymmetrical (Figure 3(c)), which indicated the presence of a mixture of clusters and NPs. When the metal loading was increased to 1.0 wt%, the IR peak at 2074 cm^{-1} became much broader (Figure 3(d)), indicative of NPs formation. Further evidence was provided by TEM analysis where NPs with an average diameter of about 3 nm were detected (Figure S4(e, f) in the Supporting Information). XRD analysis of the sample showed a small peak at 39.7° (Figure 4(a)), which was not clearly observed in two other samples at lower loading.

To provide direct evidence for the local Pt coordination structure, X-ray absorption studies were performed. Extended X-ray absorption fine structure (EXAFS) spectra (Figure 5(a)) revealed both Pt–Pt and Pt–O (or N) contributions in the 0.2 Pt-SBA-15-500 sample, indicative for significant Pt–Pt contribution. At decreased Pt loading (0.1 wt%), the sample showed higher amounts of Pt–O (or N) contribution. The weaker peak at 2.75 Å could correspond to the higher shell of Pt–O (or N)

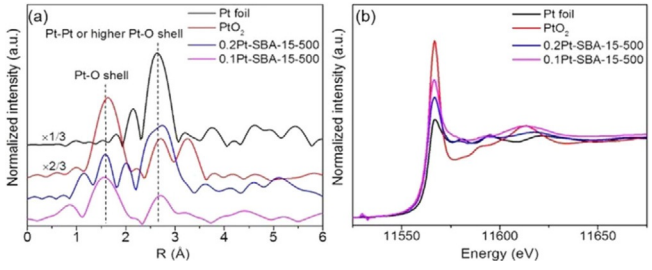

Figure 5. (a) EXAFS and (b) XANES spectra of Pt-SBA-15 materials at two different Pt loadings.

contribution as observed in the L_3-edge k-space spectra (Figure S3 in the Supporting Information).[16] Figure 2(b) shows the normalized X-ray absorption near-edge structure (XANES) spectra of the two samples, and the reference spectra of Pt foil and PtO_2. The white-line intensities in the spectra reflected the positive oxidation state of Pt in the two samples with different loadings. The Pt species in 0.1 Pt-SBA-15-500 sample carried higher positive charges, suggesting the dominance of the Pt–O (or N) contribution. At higher loading, the white-line intensity was closer to that of the Pt foil, which suggested that the sample contained Pt clusters or NPs.

To validate the effectiveness of our present methodology, controlled catalysts (designated as *x*Pt-SBA-15-*T*-C) using the H_2PtCl_6 precursor were prepared by using the same method. IR spectra of controlled catalysts at loadings of 0.3 and 1.0 wt% showed the characteristic peaks at 2063 and 2062 cm^{-1} (Figure S5(a, b) in the Supporting Information), designated as the linearly adsorbed CO on NPs. The controlled sample of 0.2 wt% Pt loading did not show any CO adsorption. XRD analysis revealed clear peaks at 39.7°, 46.2°, and 67.4° corresponding to the crystalline planes (111), (200), and (220) of Pt NPs for these samples (Figure 4(b)).[17] The peak intensities increased with Pt loading, implying increased particle sizes, which was further confirmed by TEM analysis (Figure S4(g, h) in the Supporting Information). H_2 pulse titration experiments provided the dispersion of Pt over SBA-15 in both cases. The Pt dispersion was observed to be much higher in the samples derived from Pt(TBTP) precursor compared with H_2PtCl_6 (Figure S6 in the Supporting Information).

The catalytic performance of the catalysts was tested in the hydrogenation of different functional groups. Catalysts prepared from the Pt(TBTP) complex showed very high activities compared with the catalysts prepared from H_2PtCl_6. By using a very low Pt/substrate ratio (1:4000), almost quantitative conversion could be achieved in the hydrogenation of phenylacetylene (Table S4 in the Supporting Information). At longer reaction times, the catalysts treated at 500 °C gave higher selectivity for the semi-hydrogenation product compared with the controlled catalysts. To obtain the intrinsic hydrogenation activities of the catalysts, the CS_2 poison titration method was adopted to determine the surface atom fraction (Figure S7 in the Supporting Information). Assuming that each CS_2 molecule blocked two surface Pt atoms, we determined the surface atom fraction to be 20% and 1.5% for 0.2 Pt-SBA-15-500 and 0.2 Pt-SBA-15-500-C catalysts, respectively, which was in accordance with the results obtained from the H_2 pulse titration method.

The activities of the catalysts were further verified for the hydrogenation of the -NO_2 group in nitrobenzene (Table S5 in the Supporting Information). The main purpose of selecting the hydrogenation of the -NO_2 group is to differentiate the nature of the Pt species based on the product selectivities. As the -NO_2 group is very easy to be reduced; its hydrogenation depends on many factors including both catalyst features and reaction conditions. The hydrogenation of nitrobenzene follows sequential steps to give aniline as the final product and produces different intermediates during the reaction. In fixed

reaction conditions, the product selectivity is observed to be dependent on nature of the metal, oxidation state of the metal, and acid-base property of the catalyst support. As in the present case, we use only Pt metal as the catalyst and the silica support is neutral, the product selectivity is expected to be dependent on the oxidation state of the Pt species only. Very high reaction rates were observed for the Pt-SBA-15 catalysts compared with the controlled catalysts (Pt-SBA-15-C). Notably, the product distribution was drastically different. Over Pt-SBA-15 catalysts, four different products were detected, including aniline, nitrosobenzene, azobenzene, and azoxybenzene with aniline as the major product (Table S5 in the Supporting Information). In sharp contrast, aniline was the only product obtained over Pt-SBA-15-C. This could be attributed to the presence of both positively charged single atoms as well as reduced NPs in Pt-SBA-15, which gave different intermediate products along with the target aniline. In the case of the catalyst **A** derived from the Pt(TBTP) precursor, the Pt species are slightly oxidized owing to the presence of single atoms and nanoclusters, and therefore produced significant amounts of intermediate products (such as nitrosobenzene and azoxybenzene in this case). However, in the case of controlled catalyst **A**-C, the Pt species are highly reduced owing to the formation of nanoparticles, and therefore gave the fully hydrogenation product, that is, aniline. We also compared the turnover frequency (TOF) of our catalysts with previously reported nanometric and single-atom Pt catalysts for the hydrogenation of -C≡C, -NO_2, and -C=O groups (Table 1 and Table 2). Several-fold increments of activities were observed compared with the previously reported Pt catalysts. In particular, the TOFs for -NO_2 hydrogenation were exceptionally high, which was presumably due to the presence of Pt-N species, favoring the dissociative adsorption of the reactant nitrobenzene and facilitating the desorption of the product aniline.[7]

After studying the hydrogenation of -C≡C and -NO_2 functionalities, we sought to find out the activities of our catalysts in -C=O bond hydrogenation. The experiments were carried out at high stirring speed to rule out mass transfer limitations (see Figure S8 in the Supporting Information for the effect of stirring speed). The effects of different parameters (reaction time, temperature, and H_2 pressure) were studied (Figures S9, S10, and S11 in the Supporting Information), which revealed that Pt-SBA-15 performed considerably better than Pt-SBA-15-C. Kinetic studies were also performed (Figure S12 in the Supporting Information). Both catalysts followed first-order kinetics up to a certain concentration of benzaldehyde in the presence of a fixed amount of catalyst. However, the reaction rate of Pt-SBA-15 was much higher than Pt-SBA-15-C in all experiments. The reusability of the catalyst was examined in the hydrogenation of benzaldehyde at optimized conditions; the activity was retained for up to seven consecutive cycles (Figure S13 in the Supporting Information).

Table 1. Hydrogenation of common functional groups over Pt catalysts.

Entry	Substrate	Catalyst	Major products, selectivity [%]	SA[a] [$mol_{sub}\,mol_{Pt}^{-1}\,h^{-1}$]	TOF [h^{-1}]
1[b]	PhAc	**A**	styrene, 94 ethylbenzene, 6	3888	16336
2[b]	PhAc	**A**-C	styrene, 85 ethylbenzene, 15	315	15517
3[b]	nitrobenzene	**A**	nitrosobenzene, 25 aniline, 47 azoxybenzene, 28	7552	31731
4[b]	nitrobenzene	**A**-C	aniline, 100	208	10246
5[c]	benzaldehyde	**A**	benzyl alcohol, 100	391	1643
6[c]	benzaldehyde	**A**-C	benzyl alcohol, 100	23	1133

[a] SA stands for specific activity. Reaction conditions: 2 mL methanol, 10 bar H_2. [b] Substrate/Pt = 4000, room temperature, 15 min. [c] Substrate/Pt = 500, 50 °C, 1 h. **A**: 0.2 Pt-SBA-15-500, **A**-C: 0.2 Pt-SBA-15-500-C.

Based on earlier studies on gold and iron,[23] we propose that the Pt NPs in the catalyst could be selectively dissolved in aqua regia, leaving positively charged single atoms and clusters on the support because of their stronger metal–support interaction. Indeed, Pt NPs could be selectively removed after optimization of the concentration of aqua regia. After treatment of the catalyst with 1 M aqua regia, DRIFTS results showed that the peak at 2057 cm^{-1} disappeared, corresponding to the removal of Pt NPs (Figure S14 in the Supporting Information). The new peak at 2075 cm^{-1} could be attributed to a mixture of single Pt atoms and clusters in an oxidized state. After hydrogen reduction of the sample at 200 °C, the peak shifted toward a higher value at 2085 cm^{-1} with a shoulder at

Table 2. TOF values for the hydrogenation of different functional groups over Pt-based catalysts reported previously in the literature.

Group	Substrate	Product	Catalyst	T [°C]/H_2 [bar]	Substrate/Pt	TOF [h^{-1}]	Ref
-C≡C	PhAc	styrene	Pt/KCC-1	RT/10	1950	366	[18]
	PhAc	ethylbenzene	Pt/KCC-1	RT/10	1950	73	[18]
	PhAc	styrene	Pt-PMA/AC	RT/10	1000	492	[15a]
-NO_2	4-chloronitrobenzene	4-chloroaniline	Pt-CNF-P	RT/10	1220	610	[19]
	3-nitrostyrene	3-vinylaniline	Pt-Q@IL	50/5	500	1300	[20]
	3-nitrostyrene	3-vinylaniline	Pt/FeO_x	40/3	1250	1500	[16a]
	nitrobenzene	aniline	Pt-NHCs	30/1	2000	4900	[21]
	nitrobenzene	aniline	Pt/KCC-1	RT/10	1950	325	[18]
	nitrobenzene	aniline	Pt-PMA/AC	RT/10	2000	774	[15a]
-CHO	benzaldehyde	benzyl alcohol	Pt/$MgAl_2O_4$	40/1	590	56	[22]
	4-hydroxybenzaldehyde	4-hydroxybenzyl alcohol	Pt/$MgAl_2O_4$	40/1	590	22	[22]

2076 cm^{-1}, suggesting the presence of single Pt atoms and clusters in a reduced state. After the selective leaching of Pt NPs, the catalyst showed a small decrease in specific activity, but the selectivity for the semi-hydrogenation product was increased (Tables S7 and S8 in the Supporting Information), characteristic of single-atom catalysts based on earlier studies.[13,24] The decrease in activity of the acid-leached samples could be attributed to the higher oxidation state of Pt species (Figure S14 (b vs. d) in the Supporting Information). However, the activity could be recovered after treating the sample with hydrogen as the Pt species returned to their initial oxidation state. This highlighted that our method is applicable to single-atom and sub-nanocluster catalysts on an inert support with higher metal loading by providing a simple post-leaching treatment. To gain further understanding on the mechanism of the investigated hydrogenation reactions, we plan to conduct parahydrogen-induced polarization experiments. They have been previously proven to provide insight into the pairwise hydrogen addition route on atomically dispersed[25] and nanoparticle[26] catalysts. Different reaction pathways between the platinum single-atom and sub-nanometric catalysts are possible.

Conclusions

We have presented an effective method to synthesize single-atom and sub-nanometric Pt catalysts over an inert silica support. High thermal stability of the designed Pt(TBTP) complex, and its ability to partially retain carbon and nitrogen after decomposition, were key to achieving well-dispersed, uniform Pt species on SBA-15. The advantage of the synthetic protocol was clearly proven by comparing the dispersion and catalytic activities of the new catalyst with the ones derived from a conventional simple salt precursor. The catalysts showed exceptional activities and high selectivities in the hydrogenation of different functional groups, indicating that the present method may potentially be extended to the synthesis of a series of highly active catalysts for a wide range of applications. Future research endeavors may also be directed to reveal the correlations between surface property and the single-atom/sub-nanocluster catalytic activity. For instance, the effect of the hydrophobicity/hydrophilicity of the support, which plays a critical role in nanoparticle catalysts,[27] remain to be explored in the current system.

Experimental Section

Preparation of mesoporous SBA-15 silica

Silica SBA-15 was prepared according to the method previously reported in the literature.[28] Pluronic P123 (6 g) was dissolved in water (45 g) and 2 M HCl solution (180 g) with stirring at room temperature for 30 min. Tetraethyl orthosilicate (TEOS, 12.75 g) was added to the solution with stirring at 308 K for 20 h. The mixture was aged at 363 K for 24 h. The white powder was recovered through filtration, washed with water and ethanol thoroughly, and dried in air for overnight. The product was then calcined at 873 K for 6 h to obtain SBA-15 with the Brunauer–Emmett–Teller (BET) surface area of 582 $m^2 g^{-1}$.

Preparation of [Pt(tBu$_3$tpy)Cl]Cl complex

The total synthesis was carried out in two steps by using a previously reported method.[29] To prepare the Pt(COD)Cl_2 complex, potassium tetrachloroplatinate (K_2PtCl_4, 2.00 g, 4.8 mmol) was dissolved in a solution of water (53.0 mL) and acetic acid (63.0 mL). To the light-red solution was added 1,5-cyclooctadiene (1.6 mL, 1.36 g, 12.6 mmol; COD). The reaction mixture was stirred rapidly and heated to 110 °C. Over 3 h, the solution became pale yellow and a white precipitate was formed. The volume of the solution was reduced to about 20 mL by evaporation under reduced pressure. The precipitate was collected and washed in succession with small portions of water, ethanol, and diethyl ether. The product was dried under vacuum to give white needles (1.71 g, 95% yield).

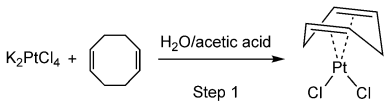

In the following step, a portion of Pt(COD)Cl_2 (286 mg, 0.76 mmol) and tBu$_3$tpy (317 mg, 0.79 mmol) were stirred in H_2O (40 mL), MeOH (15 mL), and acetone (2 mL) in air at 80 °C. A yellow solution and undissolved white reactant were evident after 12 h of stirring. After about 48 h of stirring, the solution was filtered over Celite to remove a minute amount of undissolved starting materials and the methanol and acetone were removed under vacuum. The product was extracted into CH_2Cl_2 to produce a yellow organic layer and a cloudy white aqueous layer. The CH_2Cl_2 was removed under vacuum to produce a yellow powder. The powder was washed with diethyl ether to give a yield of 93%. The product [Pt(tBu$_3$tpy)Cl]Cl was characterized by using ^{1}H NMR spectroscopy and ESI-MS, and was in agreement with the literature.[29] A purity check was carried by using elemental analysis and it was in good agreement with the predicted values (Table S3 in the Supporting Information).

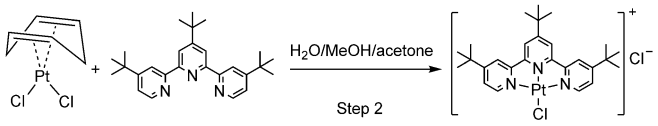

Preparation of Pt-SBA-15 catalysts from Pt(TBTP) precursor

The required amount of Pt(TBTP) complex was dissolved in methanol (5 mL) and pretreated SBA-15 (0.45 g) was added to this solution. The mixture was sonicated for 10 min and then vigorously stirred at room temperature for another 30 min. 0.5 M NaOH solution (30 μL) was added to the solution and stirring was continued for 1 h. The mixture was washed with methanol and centrifuged at 7000 rpm to collect the solid product, which was dried at 50 °C overnight. The powder sample was then treated at 500 °C for 2 h at a heating rate of 10 °C min^{-1} under N_2 atmosphere. The catalyst with x wt% Pt loading was designated as xPt-SBA-15-500.

Preparation of controlled Pt-SBA-15 catalysts from H_2PtCl_6 precursor

The required amount of H_2PtCl_6 was dissolved in methanol (5 mL) and pretreated SBA-15 (0.45 g) was added to this solution. The mixture was sonicated for 10 min and then vigorously stirred at room temperature for another 30 min. A minimum amount (μL) of

0.5 M NaOH solution was added in the solution with stirring to fully adsorb the platinum salt on SBA-15. The mixture was washed with methanol and centrifuged at 7000 rpm to collect the solid product, which was dried at 50 °C overnight. The powder sample was then treated at 500 °C for 2 h at a heating rate of 10 °C min^{-1} under N_2 atmosphere. The catalyst with *x* wt% Pt loading was designated as *x*Pt-SBA-15–500-C (C denotes controlled sample).

Selective leaching of Pt NPs

The catalyst (100 mg) was added to 1 M aqua regia (2 mL) and stirred for 12 h at room temperature. The mixture was centrifuged to separate the catalyst and the solution was analyzed by inductively coupled plasma optical emission spectrometry (ICP-OES) to determine the leached Pt amount. The catalyst was washed several times with distilled water and finally with methanol and oven dried at 50 °C overnight.

Temperature-programmed decomposition

Temperature-programmed decomposition of the catalyst precursor was measured with a Micromeritics AutoChemII 2920 instrument. Typically, the sample (30 mg) was pretreated at 50 °C in pure helium (15 mL min^{-1}) gas flow for 1 h. Subsequently, the temperature was raised from 50 to 900 °C at a rate of 10 °C min^{-1} under helium flow. The effluent gases were analyzed by using a mass spectrometer.

Hydrogen–oxygen titration

H_2–O_2 titration was conducted with a ChemBET Pulsar TPR/TPD (Quantachrome). A certain amount of catalyst was pretreated with air at 100 °C for 30 min to remove the hydrogen atoms adsorbed (if any) on Pt atoms. After that, N_2 was used as the carrier gas at 80 mL min^{-1}, and the successive doses of H_2 gas were subsequently introduced into the N_2 stream by means of a calibrated injection valve (159 μL_{H2} pulse^{-1}) at 100 °C. The titration ended when the intensities of three peaks in a row were constant. In principle, the titration should follow this equation: PtO (surface) + 3/2 H_2 = PtH (surface) + H_2O. Thus, the dispersion of Pt (d_{Pt}) should be calculated by using this formula: $d_{Pt} = 2/3\, n_{H2}/n_{total\,Pt}$.

Diffuse reflectance infrared Fourier transform spectroscopy (DRIFTS)

Diffuse reflectance infrared Fourier transform spectroscopy measurements were performed with a Thermo Scientific Nicolet iS50 FTIR spectrometer with a MCT detector, and a Praying Mantis™ high-temperature reaction chamber with ZnSe windows. The CO adsorption on Pt-SBA-15 samples was performed at room temperature. 5% CO/Ar (UHP) was introduced into the DRIFTS cell at a flow rate of 40 mL min^{-1}. After the CO saturation, a N_2 purge at a flow rate of 40 mL min^{-1} was performed to remove gas-phase CO from the DRIFTS cell and then the adsorbed CO on Pt. All the spectra were recorded by using 32 scans and a resolution of 4 cm^{-1}.

Transmission electron microscopy

Transmission electron microscopy (TEM) was performed with a JEM 2100F (JEOL, Japan) microscope operated at 200 kV. X-ray diffraction (XRD) analysis was carried out by using a Bruker D8 Advance X-Ray Diffractometer, at a scan rate of 3° min^{-1}. It was operated at 40 kV, applying a potential current of 30 mA. X-ray photoelectron spectra (XPS) were recorded with a VG Escalab MKII spectrometer, using a mono $Al_{K\alpha}$ X-ray source ($h\nu$ = 1486.71 eV, 5 mA, 15 kV), and the calibration was done by setting the C 1s peak at 284.5 eV. Electrospray ionization (ESI) mass spectrometric analysis was performed with a Bruker microTOF-Q system. Thermogravimetric analysis was conducted with a DTG-60A thermogravimetry analyzer (Shimadzu) under a nitrogen atmosphere. The Pt content in the catalysts was determined by using an iCAP 6000 series inductively coupled plasma optical emission spectrometer (ICP-OES). Gas chromatography (GC) analysis was done by using an Agilent 7890C GC equipped with a HP-5 column and a flame ionization detector (FID) detector.

X-ray absorption spectroscopy

Pt L_3-edge X-ray absorption spectra (XAS) of supported catalysts and references (Pt foil and PtO_2) were recorded at the BL01B1 beamline at the Spring-8 (Japan Synchrotron Radiation Research Institute, Hyogo, Japan) in the transmission mode at ambient temperature. Data analysis was carried out with Athena and Artemis included in the Ifeffit and Demeter package. For curve-fitting analysis on extended X-ray absorption fine structure (EXAFS) spectra, each theoretical scattering path was generated with FEFF 6.0 L. The k^3-weighted EXAFS oscillation in the range of 3.0–13 Å^{-1} was Fourier transformed.

Hydrogenation of phenylacetylene

The required amounts of phenylacetylene, catalyst, and solvent were charged into a 20 mL autoclave reactor. The reactor was then flushed with purified H_2 three times and finally filled with 10 bar of H_2. The reaction was performed at room temperature with a stirring speed of 1000 rpm. After completion of the reaction, the H_2 pressure was released and products were analyzed by GC.

Hydrogenation of benzaldehyde

The required amounts of benzaldehyde, catalyst, and solvent were charged into a 20 mL autoclave reactor. The reactor was then flushed with purified H_2 three times and finally filled with 10 bar of H_2. The reaction was performed at the desired temperature in a pre-heated oil bath with a stirring speed of 1000 rpm. After completion of the reaction, the reactor was cooled down to room temperature and the H_2 pressure was released, and products were analyzed by GC.

Hydrogenation of nitrobenzene

The required amounts of nitrobenzene, catalyst, and solvent were charged into a 20 mL autoclave reactor. The reactor was then flushed with purified H_2 three times and finally filled with 10 bar of H_2. The reaction was performed at room temperature with a stirring speed of 800 rpm. After completion of the reaction, the H_2 pressure was released and products were analyzed by GC.

Catalytic recycling experiment for the hydrogenation of benzaldehyde

Catalyst (54 mg), benzaldehyde (14.1 μL), and methanol (2 mL) were charged into a 20 mL autoclave reactor. The reactor was then flushed with purified H_2 three times and finally filled with 10 bar of H_2. The reaction was performed at 50 °C for 1 h in a pre-heated oil bath with a stirring speed of 1000 rpm. After completion of the reaction, the reactor was cooled down to room temperature and the H_2 pressure was released, and products were analyzed by GC. The

spent catalyst was thoroughly washed with methanol and then used for the next catalytic run.

Acknowledgments

The authors gratefully acknowledge the Young Researcher Award from the National University of Singapore (WBS: R-279-000-464-133), MOE Tier-2 grant (WBS: R-279-000-462-112), and MOE Tier-1 grant (R-279-000-438-112).

Conflict of interest

The authors declare no conflict of interest.

Keywords: heterogeneous catalysis · hydrogenation · nanocatalysis · single-atom catalysis · supported catalysis

[1] a) K. Mori, T. Hara, T. Mizugaki, K. Ebitani, K. Kaneda, *J. Am. Chem. Soc.* **2004**, *126*, 10657 – 10666; b) J. Huang, T. Akita, J. Faye, T. Fujitani, T. Takei, M. Haruta, *Angew. Chem. Int. Ed.* **2009**, *48*, 7862 – 7866; *Angew. Chem.* **2009**, *121*, 8002 – 8006; c) M. D. Rossell, F. J. Caparros, I. Angurell, G. Muller, J. Llorca, M. Seco, O. Rossell, *Catal. Sci. Technol.* **2016**, *6*, 4081 – 4085; d) Z. Zhang, Y. Zhu, H. Asakura, B. Zhang, J. Zhang, M. Zhou, Y. Han, T. Tanaka, A. Wang, T. Zhang, N. Yan, *Nat. Commun.* **2017**, *8*, 16100; e) X.-F. Yang, A. Wang, B. Qiao, J. Li, J. Liu, T. Zhang, *Acc. Chem. Res.* **2013**, *46*, 1740 – 1748; f) J. Liu, *ACS Catal.* **2017**, *7*, 34 – 59; g) B. C. Gates, M. Flytzani-Stephanopoulos, D. A. Dixon, A. Katz, *Catal. Sci. Technol.* **2017**, *7*, 4259 – 4275.

[2] a) M. Rivallan, E. Seguin, S. Thomas, M. Lepage, N. Takagi, H. Hirata, F. Thibault-Starzyk, *Angew. Chem. Int. Ed.* **2010**, *49*, 785 – 789; *Angew. Chem.* **2010**, *122*, 797 – 801; b) J. Zečević, A. M. J. van der Eerden, H. Friedrich, P. E. de Jongh, K. P. de Jong, *ACS Nano* **2013**, *7*, 3698 – 3705.

[3] a) B. S. Lim, A. Rahtu, R. G. Gordon, *Nat. Mater.* **2003**, *2*, 749 – 754; b) A. Meffre, B. Mehdaoui, V. Kelsen, P. F. Fazzini, J. Carrey, S. Lachaize, M. Respaud, B. Chaudret, *Nano Lett.* **2012**, *12*, 4722 – 4728; c) T. Hyeon, *Chem. Commun.* **2003**, 927 – 934.

[4] B. C. Gates, *Chem. Rev.* **1995**, *95*, 511 – 522.

[5] a) L. Zhang, A. Wang, W. Wang, Y. Huang, X. Liu, S. Miao, J. Liu, T. Zhang, *ACS Catal.* **2015**, *5*, 6563 – 6572; b) W. Liu, L. Zhang, W. Yan, X. Liu, X. Yang, S. Miao, W. Wang, A. Wang, T. Zhang, *Chem. Sci.* **2016**, *7*, 5758 – 5764; c) D. Deng, X. Chen, L. Yu, X. Wu, Q. Liu, Y. Liu, H. Yang, H. Tian, Y. Hu, P. Du, R. Si, J. Wang, X. Cui, H. Li, J. Xiao, T. Xu, J. Deng, F. Yang, P. N. Duchesne, P. Zhang, J. Zhou, L. Sun, J. Li, X. Pan, X. Bao, *Sci. Adv.* **2015**, *1*, e1500462; d) X. Cui, J. Xiao, Y. Wu, P. Du, R. Si, H. Yang, H. Tian, J. Li, W.-H. Zhang, D. Deng, X. Bao, *Angew. Chem. Int. Ed.* **2016**, *55*, 6708 – 6712; *Angew. Chem.* **2016**, *128*, 6820 – 6824.

[6] a) L. Fan, P. F. Liu, X. Yan, L. Gu, Z. Z. Yang, H. G. Yang, S. Qiu, X. Yao, *Nat. Commun.* **2016**, *7*, 10667; b) P. Yin, T. Yao, Y. Wu, L. Zheng, Y. Lin, W. Liu, H. Ju, J. Zhu, X. Hong, Z. Deng, G. Zhou, S. Wei, Y. Li, *Angew. Chem. Int. Ed.* **2016**, *55*, 10800 – 10805; *Angew. Chem.* **2016**, *128*, 10958 – 10963.

[7] P. Chen, A. Khetan, F. Yang, V. Migunov, P. Weide, S. P. Stürmer, P. Guo, K. Kähler, W. Xia, J. Mayer, H. Pitsch, U. Simon, M. Muhler, *ACS Catal.* **2017**, *7*, 1197 – 1206.

[8] B. Qiao, A. Wang, X. Yang, L. F. Allard, Z. Jiang, Y. Cui, J. Liu, J. Li, T. Zhang, *Nat. Chem.* **2011**, *3*, 634 – 641.

[9] a) J. H. Kwak, J. Hu, D. Mei, C.-W. Yi, D. H. Kim, C. H. F. Peden, L. F. Allard, J. Szanyi, *Science* **2009**, *325*, 1670 – 1673; b) M. Moses-DeBusk, M. Yoon, L. F. Allard, D. R. Mullins, Z. Wu, X. Yang, G. Veith, G. M. Stocks, C. K. Narula, *J. Am. Chem. Soc.* **2013**, *135*, 12634 – 12645.

[10] a) C. Wang, X.-K. Gu, H. Yan, Y. Lin, J. Li, D. Liu, W.-X. Li, J. Lu, *ACS Catal.* **2017**, *7*, 887 – 891; b) J. Jones, H. Xiong, A. T. DeLaRiva, E. J. Peterson, H. Pham, S. R. Challa, G. Qi, S. Oh, M. H. Wiebenga, X. I. Pereira Hernández, Y. Wang, A. K. Datye, *Science* **2016**, *353*, 150 – 154.

[11] a) T.-Y. Chang, Y. Tanaka, R. Ishikawa, K. Toyoura, K. Matsunaga, Y. Ikuhara, N. Shibata, *Nano Lett.* **2014**, *14*, 134 – 138; b) J. C. Matsubu, S. Zhang, L. DeRita, N. S. Marinkovic, J. G. Chen, G. W. Graham, X. Pan, P. Christopher, *Nat. Chem.* **2017**, *9*, 120 – 127.

[12] R. Lang, T. Li, D. Matsumura, S. Miao, Y. Ren, Y.-T. Cui, Y. Tan, B. Qiao, L. Li, A. Wang, X. Wang, T. Zhang, *Angew. Chem. Int. Ed.* **2016**, *55*, 16054 – 16058; *Angew. Chem.* **2016**, *128*, 16288 – 16292.

[13] a) G. Vilé, D. Albani, M. Nachtegaal, Z. Chen, D. Dontsova, M. Antonietti, N. López, J. Pérez-Ramírez, *Angew. Chem. Int. Ed.* **2015**, *54*, 11265 – 11269; *Angew. Chem.* **2015**, *127*, 11417 – 11422; b) X. Huang, Y. Xia, Y. Cao, X. Zheng, H. Pan, J. Zhu, C. Ma, H. Wang, J. Li, R. You, S. Wei, W. Huang, J. Lu, *Nano Res.* **2017**, *10*, 1302 – 1312.

[14] a) S. Yang, J. Kim, Y. J. Tak, A. Soon, H. Lee, *Angew. Chem. Int. Ed.* **2016**, *55*, 2058 – 2062; *Angew. Chem.* **2016**, *128*, 2098 – 2102; b) S. Yang, Y. J. Tak, J. Kim, A. Soon, H. Lee, *ACS Catal.* **2017**, *7*, 1301 – 1307.

[15] a) B. Zhang, H. Asakura, J. Zhang, J. Zhang, S. De, N. Yan, *Angew. Chem. Int. Ed.* **2016**, *55*, 8319 – 8323; *Angew. Chem.* **2016**, *128*, 8459 – 8463; b) B. Zhang, H. Asakura, N. Yan, *Ind. Eng. Chem. Res.* **2017**, *56*, 3578 – 3587.

[16] a) H. Wei, X. Liu, A. Wang, L. Zhang, B. Qiao, X. Yang, Y. Huang, S. Miao, J. Liu, T. Zhang, *Nat. Commun.* **2014**, *5*, 5634; b) J. C. Matsubu, V. N. Yang, P. Christopher, *J. Am. Chem. Soc.* **2015**, *137*, 3076 – 3084.

[17] F. Sen, Y. Karatas, M. Gulcan, M. Zahmakiran, *RSC Adv.* **2014**, *4*, 1526 – 1531.

[18] M. Dhiman, V. Polshettiwar, *J. Mater. Chem. A* **2016**, *4*, 12416 – 12424.

[19] M. Takasaki, Y. Motoyama, K. Higashi, S.-H. Yoon, I. Mochida, H. Nagashima, *Org. Lett.* **2008**, *10*, 1601 – 1604.

[20] M. J. Beier, J.-M. Andanson, A. Baiker, *ACS Catal.* **2012**, *2*, 2587 – 2595.

[21] P. Lara, A. Suárez, V. Collière, K. Philippot, B. Chaudret, *ChemCatChem* **2014**, *6*, 87 – 90.

[22] M. Han, H. Zhang, Y. Du, P. Yang, Z. Deng, *Reac. Kinet. Mech. Cat.* **2011**, *102*, 393 – 404.

[23] P. Schwach, M. G. Willinger, A. Trunschke, R. Schlögl, *Angew. Chem. Int. Ed.* **2013**, *52*, 11381 – 11384; *Angew. Chem.* **2013**, *125*, 11591 – 11594.

[24] a) G. Kyriakou, M. B. Boucher, A. D. Jewell, E. A. Lewis, T. J. Lawton, A. E. Baber, H. L. Tierney, M. Flytzani-Stephanopoulos, E. C. H. Sykes, *Science* **2012**, *335*, 1209 – 1212; b) G. X. Pei, X. Y. Liu, X. Yang, L. Zhang, A. Wang, L. Li, H. Wang, X. Wang, T. Zhang, *ACS Catal.* **2017**, *7*, 1491 – 1500.

[25] A. Corma, O. G. Salnikov, D. A. Barskiy, K. V. Kovtunov, I. V. Koptyug, *Chem. Eur. J.* **2015**, *21*, 7012 – 7015.

[26] a) R. Zhou, W. Cheng, L. M. Neal, E. W. Zhao, K. Ludden, H. E. Hagelin-Weaver, C. R. Bowers, *Phys. Chem. Chem. Phys.* **2015**, *17*, 26121 – 26129; b) R. Zhou, E. W. Zhao, W. Cheng, L. M. Neal, H. Zheng, R. E. Quiñones, H. E. Hagelin-Weaver, C. R. Bowers, *J. Am. Chem. Soc.* **2015**, *137*, 1938 – 1946.

[27] a) Y. Kuwahara, T. Kamegawa, K. Mori, H. Yamashita, *Chem. Commun.* **2008**, 4783 – 4785; b) Y. Kuwahara, H. Yamashita, *J. Mater. Chem.* **2011**, *21*, 2407 – 2416.

[28] D. Zhao, Q. Huo, J. Feng, B. F. Chmelka, G. D. Stucky, *J. Am. Chem. Soc.* **1998**, *120*, 6024 – 6036.

[29] a) A. Tronnier, A. Poethig, E. Herdtweck, T. Strassner, *Organometallics* **2014**, *33*, 898 – 908; b) F. G. Baddour, M. I. Kahn, J. A. Golen, A. L. Rheingold, L. H. Doerrer, *Chem. Commun.* **2010**, *46*, 4968 – 4970.

Manuscript received: January 23, 2018
Revised manuscript received: February 20, 2018
Accepted manuscript online: February 21, 2018
Version of record online: March 23, 2018